Giant magnetic modulation of a planar, hybrid metamolecule resonance

2014 New J. Phys. 16 063002

(http://iopscience.iop.org/1367-2630/16/6/063002)

New Journal of Physics
The open access journal at the forefront of physics
Deutsche Physikalische Gesellschaft DPG | IOP Institute of Physics

Giant magnetic modulation of a planar, hybrid metamolecule resonance

Simon A Gregory[1], Gavin B G Stenning[1], Graham J Bowden[1], Nikolay I Zheludev[2,3] and Peter A J de Groot[1]

[1] Physics & Astronomy and Centre for Photonic Metamaterials, University of Southampton, Southampton SO17 1BJ, UK
[2] Optoelectronics Research Centre and Centre for Photonic Metamaterials, University of Southampton, Southampton SO17 1BJ, UK
[3] Centre for Disruptive Photonic Technologies, NTU, Singapore 637371, Singapore
E-mail: s.gregory@soton.ac.uk

Received 3 January 2014, revised 15 April 2014
Accepted for publication 25 April 2014
Published 3 June 2014

New Journal of Physics **16** (2014) 063002

doi:10.1088/1367-2630/16/6/063002

Abstract

Coupling magnetic elements to metamaterial structures creates hybrid metamolecules with new opportunities. Here we report on the magnetic control of a metamolecule resonance, by utilizing the interaction between a single split ring resonator (SRR) and a magnetic thin film of permalloy. To suppress eddy current shielding, the permalloy films are patterned into arrays of 30–500 μm diameter discs. Strong hybridized resonances were observed at the anticrossing between the split ring resonance and the ferromagnetic resonance (FMR) of the permalloy. In particular, it is possible to achieve 40 dB modulation of the electric (symmetric) mode of the SRR on sweeping the applied magnetic field through the SRR/FMR anticrossing. The results open the way to the design of planar metamaterials, with potential applications in nonlinear metamaterials, tunable metamaterials and spintronics.

S Online supplementary data available from stacks.iop.org/NJP/16/063002/mmedia

Keywords: metamaterials, permalloy, hybrid metamaterials, coplanar waveguide

1. Introduction

Electromagnetic metamaterials, characterized by sub-wavelength length scales, have attracted much attention in recent years due to the control of light that they allow. In particular, the dispersion properties of metamaterials have been manipulated to access unusual permittivities and permeabilities leading to negative index of refraction [1, 2], zero epsilon [3], giant chirality [4], and hyperbolic dispersion anisotropy [5]. Metamaterials have been designed with highly unusual properties, such as invisible metallic structures [6], extraordinary resonant transparency [7–10], perfect absorption [6, 11, 12] and magnetic mirrors [13, 14]. They can also be configured to perform waveform manipulation [15], and offer exciting opportunities for cloaking, waveguiding, and localization of light [16, 17].

More recently, there has been a concerted effort to build on the success of passive metamaterials via the development of active metamaterials. These have functionalities which can be externally controlled to modify metamaterial response in the time domain. Metamaterials have already been exploited to enhance nonlinear switching [18] and light emission performance of conventional active materials [19, 20]. Such varied technological prospects have stimulated new searches for metamaterials with tunable and/or switchable properties using MEMS, semiconductors, phase change media, liquid crystals, superconductors and magnetic media [15, 21, 22]. In particular, magnetic materials have the potential to add a large range of nonlinear functionalities to metamaterials, given the inherent nonlinear properties of magnetic media.

To date magnetic hybrid metamaterial research has focussed on coupling ohmic metamaterial structures with resonant magnetic material [12, 23–30]. This work has been performed using ferrites, predominantly the ferrimagnetic material yttrium iron garnet (YIG), notable for its low-loss magnetic resonance behaviour and wide use in microwave electronics [23, 31, 32]. In practice, the majority of these experiments have been carried out at relatively low frequencies (~10 GHz) using cavity waveguides and bulk YIG single crystals [23–25, 28]. An exception is the recent experiment reported by Stenning *et al* [23], which employs a broadband coplanar arrangement loaded with a thin YIG film and a split ring resonator (SRR). Here, a coplanar waveguide (CPW) was used to excite the hybrid SRR/YIG system and allowing it to be studied in a comprehensive fashion. Such planar device structures lend themselves to applications in microwave electronics [33–35]. However, YIG and other ferrites are restricted in their application because of their limited frequency range (typically less than 10 GHz) and they are hard to pattern or grow as magnetic multilayers. In contrast, over the last 25 years the development of materials and devices based on transition-metal magnetic films has undergone a revolution. Metallic magnetic films can be patterned easily to micron and sub-micron length scales and grown as bilayers or multilayers. They also allow access to a rich variety of magnetic phenomena such as magnetic exchange bias (with associated high-frequency exchange resonance modes), spintronics, resonances in geometrically confined structures (*e.g.* magnetic vortex states), and the recently discovered range of magnonic functionalities [36, 37].

In this article we describe the development of magnetic hybrid metamaterial, this time based on transition-metal magnetic films. Permalloy ($Ni_{81}Fe_{19}$) is a transition-metal alloy well known for its low magnetic losses. Ferromagnetic resonance (FMR) is the uniform magnetic resonance mode employed in this study. During FMR, the magnetization (M) aligns to an applied field (B_a), while an excitation field is applied orthogonal to B_a. This results in the

precession of M around B_a. The frequency of rotation (ω) for a thin film magnetized in-plane is given by the Kittel formula [38]:

$$\omega = \gamma\sqrt{B_a\left(B_a + \mu_0 M\right)}. \tag{1}$$

Here γ is the gyromagnetic ratio and M is the magnetization. Metamaterial control is achieved by simultaneously exciting both the SRR resonance and FMR resonance. Since the FMR resonance depends on the strength of the applied field, it is possible to magnetically modulate the strength of the SRR resonance. FMR is well understood and may be tailored to application: the simple thin film resonance of equation (1) may be altered to include either shape anisotropy terms, from patterning [39], and/or crystalline anisotropy terms.

Continuous metallic films cannot be used in magnetic hybrid metamaterials. Induced eddy currents in the conducting films simply screen out any metamolecule resonances. However, by patterning the metallic magnetic films into small discs, eddy currents can be substantially reduced, allowing magnetic hybrid metamaterial behaviour to be achieved. These results show how the fields of metamaterials and magnonics can be combined, presenting new opportunities. While our principal aim is to create novel metamaterials, we also suggest a new method to enhance magnetic resonance effects using metamolecules (e.g. FMR) [40] with potential relevance for sensor applications. Finally, we note that while results are only presented for a single metamolecule, the essential functionalities discussed here also apply to conventional metamaterials.

2. Methods

2.1. Sample fabrication

Samples consisting of patterned permalloy films and copper SRRs, were fabricated in the clean-room facilities at the University of Southampton. A 150 nm film of $Ni_{81}Fe_{19}$ (permalloy) was deposited on a glass substrate by e-beam evaporation. It was subsequently patterned into 100 μm diameter discs using photolithography techniques. An 8 μm SU-8 insulating layer was then spun and cured onto the patterned permalloy. SU-8 is an epoxy-based negative photoresist, commonly used in MEMS. It possesses good mechanical properties able to withstand subsequent deposition and etching processes. Next, a 300 nm layer of copper was deposited on top of the SU-8 layer and subsequently patterned into a SRR structure, again by e-beam evaporation and photolithography. Finally, a 1.3 μm layer of photoresist (S1813) was spun and baked on top of the SRR, to prevent electrical contact between the SRR and the CPW during experiments. A photograph of one such sample can be seen in figure 1(a).

Two different CPW designs were used to investigate hybrid metamolecule systems. Both CPWs were designed to have 50 Ω impedance up to 20 GHz, with a signal line of 1.1 mm and gaps of 0.2 mm. The first CPW had the ground plane on the topside of the CPW connected to copper backing on its underside by vias, to improve its transmission properties and high-frequency response [41]. This 'grounded' CPW was used to investigate multilayer assemblies incorporating both a SRR and patterned permalloy. The second 'ungrounded' CPW did not have copper backing on its underside, but had a 70 μm thick copper SRR instead (figure 1(b)). This was to fix the SRR with respect to the CPW rf-fields, allowing comparative measurements between differing patterned permalloy films. The transmission characteristics of this CPW were

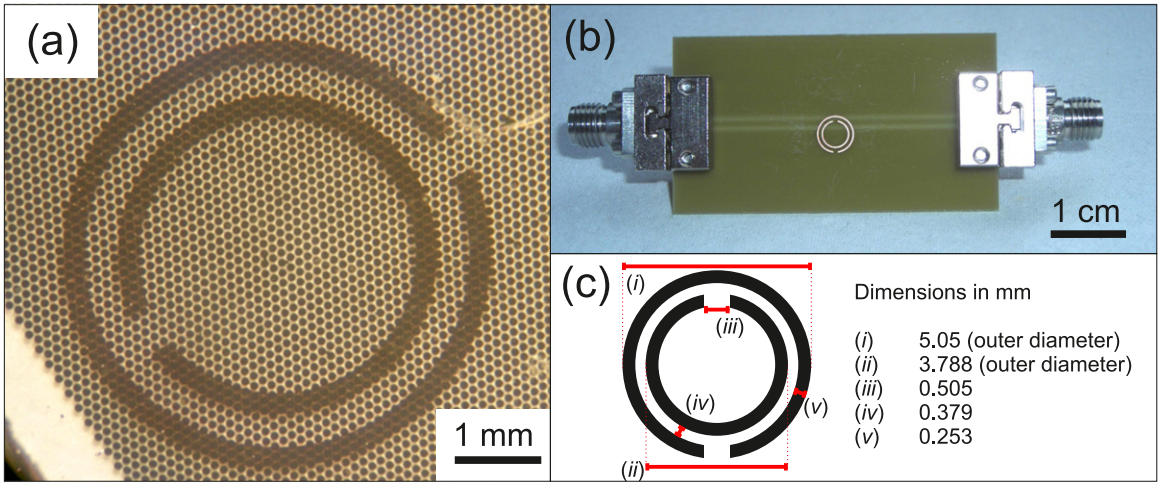

Figure 1. (a) Optical microscope image of a hybrid metamolecule, taken through the glass substrate. In the foreground are the patterned permalloy dots, and in the background the copper SRR. The sample was placed on the grounded coplanar waveguide this way up, with the SRR side facing the CPW. (b) SRR printed on the underside of an ungrounded CPW. The SRR is 70 μm thick, and is deposited on the circuit board material (FR4) 0.7 mm away from the plane of the waveguide. The gaps of the CPW are visible through the FR4. This waveguide was used to investigate different patterned permalloy films. (c) The dimensions of the SRR geometry used throughout this communication.

inferior to the grounded CPW, but sufficient for the task. Both CPWs were fabricated using simple mask/photo-etching techniques.

Permalloy films with different sized patterned discs were fabricated, to investigate the dependence of eddy current losses on element size. Arrays of discs with diameters 30, 50, 100, 200, 300, 400 and 500 μm were made, with the spacing between the discs fixed at 20 μm. The hybridization of these samples with the SRR was investigated using the ungrounded CPW shown in figure 1(b). Note that for the arrays with small discs, there is a notable decrease in filling factor.

Finally, we observe that the multilayer approach employed here is unique in magnetic hybrid metamaterials, and offers significant advantages. Not only does it allow the use of transition-metal magnetic films with engineered properties, but the multilayer assembly can be extended to include additional metamolecules and magnetic films, either in-plane or by adding more layers. The compatibility with standard cleanroom processing techniques allows highly complex planar metamaterial structures to be produced in a scalable way. This approach could also be extended to include 'layer-by-layer' methods of fabricating three dimensional (3D) metamaterials [17, 42], but this time with magnetic components.

2.2. Experimental procedures

The SRR/permalloy multilayer assemblies (see figure 1(a)) were placed on a grounded CPW in a 'flip-chip' configuration [23, 43]. This arrangement ensured good coupling between all three principal components, with the SRR separated from the CPW by only a thin (1.3 μm) layer of photoresist, and the permalloy separated from the SRR by the 8 μm SU-8 layer. The CPW, plus

multilayer assembly, was subsequently placed in an electromagnet and connected to a vector network analyzer (VNA) (HP E5071C), as in the commonly used technique of VNA-FMR [43–45]. The cables connecting the CPW to the VNA were passed through holes drilled through the two magnet pole pieces. This geometry ensures that rf magnetic fields from the CPW are perpendicular to the applied magnetic field. The magnetic field strength was measured using a Lakeshore 425 Gaussmeter. Fields of up to 0.6 T were applied while the frequency was swept from 300 kHz to 20 GHz.

During resonance of the hybrid metamolecule system, absorption and/or scattering of the rf-field causes changes in the impedance/transmission of the CPW. These changes are detected by the VNA and stored in the form of a 2×2 scattering matrix, $\boldsymbol{S}$. In practice, the transmission parameter S_{21} is most commonly used in VNA-FMR experiments [23, 43–45]. By sweeping both the frequency (ν) and the magnetic field (B_a), 2D S_{21} maps of ν versus B_a can be obtained. To highlight changes brought about by the magnetic field, the S_{21} scans were often normalized by subtracting a S_{21} scan obtained at a field far away from any magnetic resonances. The normalized field-dependent transmission parameter is denoted S_{12}^{N}.

Experiments designed to determine an optimum diameter for the permalloy discs were performed using the ungrounded CPW depicted in figure 1(b). Patterned permalloy films were placed in the flip-chip configuration on the SRR, as described by Stenning *et al* [23]. This has the advantage of allowing differing samples to be investigated with ease and reproducibility. However, the strength of coupling between three primary components is not as strong as that obtained using the metamolecule arrangement depicted in figure 1(a). In addition, because the response of ungrounded CPW falls away sharply at frequencies above ~10 GHz, the magnetic mode (~4 GHz) of the SRR was selected for the disc size experiments. However, the magnetic mode showcases the same overall trends as that obtained using the electric mode. Finally, we note that the SRR resonances in the ungrounded CPW geometry occur at lower frequencies than those obtained using the grounded CPW. The magnetic mode is shifted down from 6 GHz to 3.7 GHz, and the electric mode from 17 GHz to 13.5 GHz. This shift is probably due to the increase in local capacitance due to the FR4 circuit board substrate ($\varepsilon_r = 4.5$).

3. Giant magnetic modulation of a metamolecule resonance

A schematic of the principal experiment is displayed in figure 2. The permalloy was patterned into discs of 100 μm diameter to suppress eddy current losses, as discussed in section 4.

The resonant components of the experiment, namely the patterned permalloy and the metamolecule, are driven by the broadband CPW positioned in the electromagnet. Oscillating currents in the SRR also interact with the resonant magnetic material: the two are inductively coupled. As the FMR frequency approaches the SRR frequency (with increasing applied magnetic field), the FMR profoundly modifies the SRR resonance. This is evident from the data shown in figure 3, detailing magnetic metamolecule response in the region of the SRR electric (symmetric) mode [46, 47]. The metamolecule was placed on the CPW at a position which strongly excites this particular electric mode. The optimum position was determined empirically, and indicated in figure 2. In agreement with earlier work [23, 27], we find that the FMR couples much more strongly to the higher frequency SRR electric (symmetric) mode than the fundamental magnetic (asymmetric) mode.

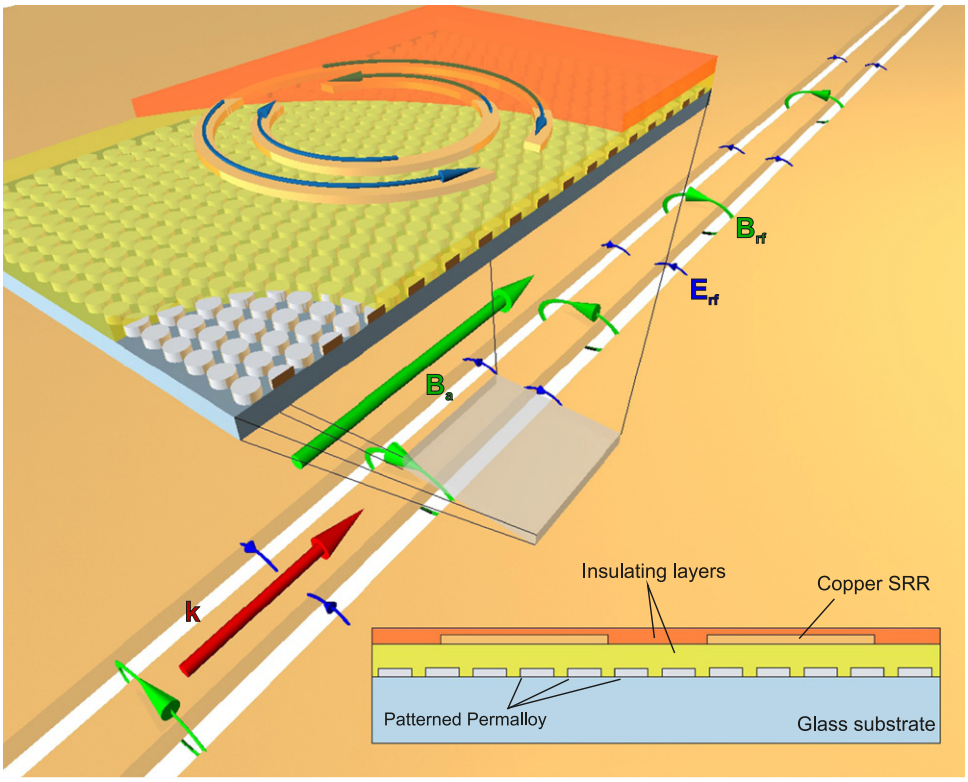

Figure 2. Schematic of a hybrid metamolecule and its placement on a coplanar waveguide, showing the resonant excitation of the metamolecule. Multilayer sample placement on the CPW is indicated by the shadow box. Also shown are arrows denoting applied dc magnetic field ($\boldsymbol{B_a}$) microwave propagation ($\boldsymbol{k}$), and CPW fields ($\boldsymbol{E_{rf}}$ and $\boldsymbol{B_{rf}}$). The latter excite current oscillations in the SRR, as indicated by the blue arrows on the SRR, and induce FMR in the magnetic material. Inset is a cross-sectional view through the multilayer. Note that during the experiments, the sample was placed the other way up (flip-chip configuration).

Figure 3 shows giant magnetic modulation of a hybrid metamolecule resonance in a planar system. The unmodulated transmission is given by the S_{21} transmission curve at $B_a = 0$ (black) in figure 3(a), with the SRR resonance unhindered. The S_{21} curve for $B_a = B_{co}$ (red) shows the maximal magnetic modulation of the system, with the relative transmission vastly increased, by 40 dB. This corresponds to the interruption of the SRR electric mode by the FMR of the permalloy. The S_{11} reflection curve (blue) shows no observable change at the SRR resonance at the scale in the figure, the FMR absorption is too small (it was observed not to exceed 0.5 dB). An animation of the modulation of the SRR resonance amplitude is provided in the supplementary information.

Figure 3(b) shows a 2D ν versus B_a map of S_{12}^N. The data reveals very strong anticrossing between the SRR and FMR resonances. This map is very similar, though much stronger in magnitude, to that obtained using YIG-metamaterial hybrids [23]. All the features of anticrossing are present: namely the Fano-like resonance shape, the change in resonance line shape on either side of the anticrossing, the shifting of the SRR resonance peak by 0.25 GHz (tunability) and the reduction in microwave losses in the frequency range either side of the

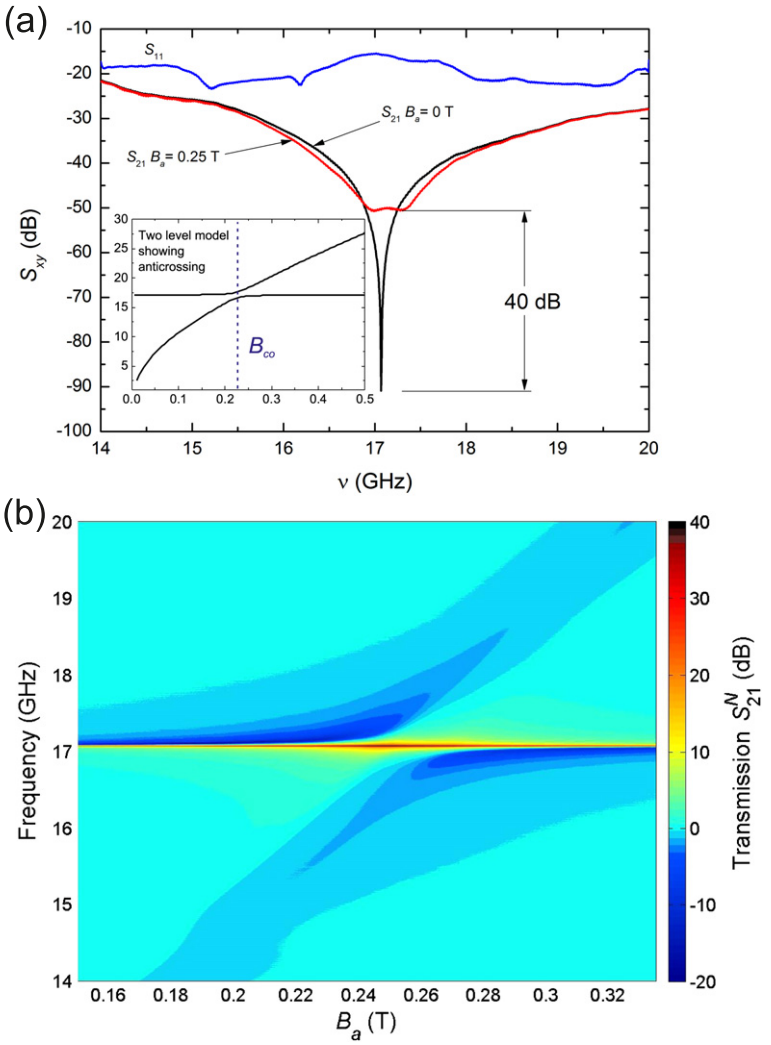

Figure 3. Modulation of a metamolecule resonance through applied magnetic field. (a) Resonant reflection and transmission characteristics of the planar waveguide loaded with an SRR hybridized with a permalloy layer. The red curve shows S_{21} at the field at which the FMR intersects the peak of the SRR resonance (the cross over field, B_{co}), resulting in a dramatic reduction of the peak amplitude, by 40 dB, compared to the S_{21} curve at 0 T (black). Inset (a): ν plotted against B_a from a simple 2-level model incorporating the FMR and SRR resonances displaying 'anticrossing' behaviour, following [23, 48]. Such anticrossing features are general phenomena for coupled oscillators. The position of B_{co} is shown by the dashed line. (b) ν-B_a map of S_{12}^N, showing the change in the SRR resonance as the near-linear FMR $\nu(B_a)$ curve intersects the horizontal SRR resonance, resulting in anticrossing. The data is normalized to a scan at zero field.

anticrossing. These results clearly demonstrate that YIG-type functionalities can be obtained with patterned transition metal films, thereby avoiding the serious limitations of working with YIG. Note also that the frequency of 17 GHz is the highest operating frequency of a magnetic hybrid metamolecule reported to date.

Lastly, we note that the results displayed here have relevance for applications in microwave components and sensors. The transmission characteristics in figure 3(a) are comparable to CPW-based passive stop-band metamolecule devices [33, 34]. In essence, the system described here can be regarded as a magnetically controllable stop-band/bandpass filter. Additionally, SRRs could be used as an enhancement tool in CPW-based VNA-FMR, for sensing applications. In conventional FMR (e.g. X-band) resonant cavities are often used to boost the FMR signal. In planar FMR, the SRR is used in place of a resonant cavity. Together with the huge dynamic range of VNAs, SRRs could be used boost sensitivity to FMR by several orders of magnitude. In addition, the compact nature of the planar system lends itself to applications in those experiments where space is at a premium (e.g. low temperature, high vacuum).

4. Varying patterned element size

The patterning of the magnetic material is the key element in eliciting hybrid phenomena using transition metal elements. If continuous metallic magnetic films are used, no SRR/FMR hybridization is observed. The effect of permalloy disk-size on hybrid metamolecule response was therefore investigated, using the ungrounded CPW and SRR shown in figure 1(b) and samples containing only the patterned permalloy dots. In these experiments, the field was fixed at a crossover field $B_{co} \approx 0.01$ T, appropriate for the magnetic mode of the SRR (~4 GHz). The frequency was subsequently scanned from 2.8 to 4.4 GHz, providing S_{12}^{N} versus (ν-B_a) maps for each permalloy array. The results are summarized in figure 4.

The black curve, at the front of figure 4, is that obtained using a continuous film. The only field-dependent feature observed is a weak FMR signal, arising from the poor coupling between the permalloy and the CPW. Any SRR resonance is simply screened out by the presence of the continuous metal film. However, when the film is patterned into disks, eddy currents are reduced and SRR/FMR hybridization occurs. The hybridization strength appears to reach a maximum for a disk size of 100 μm, indicating that an optimal size has been reached. For disk sizes smaller than 100 μm, the strength of the SRR/FMR hybridization falls due to a decrease in magnetic filling factor.

There is further scope for increasing the coupling between the magnetic material and the SRR. The resonant magnetic material and SRR interact by mutual rf-fields, generated by the oscillating currents in the SRR and out-of-plane FMR magnetization components. In the case of the magnetic SRR mode, the currents in the SRR give rise to an oscillating magnetic dipole, when viewed from far-field. However in the case of the electric SRR mode, the two symmetric current oscillations generate two opposing magnetic dipoles which cancel when viewed from a distance. Nonetheless, individual NiFe patterned elements are sufficiently close to the SRR to allow near-field FMR [37]. The mutual interaction strength between the SRR and FMR would increase when the out-of-plane magnetic fields are more concentrated, given that the FMR signal strength scales as B_{rf}^2. This provides a clear route to optimizing the strength of the coupling between the SRR and FMR. It could be increased either by optimizing the filling factor, and/or by using a material with more favourable FMR properties (lower losses/greater out-of-plane magnetization component) and/or by clever SRR placement and geometry.

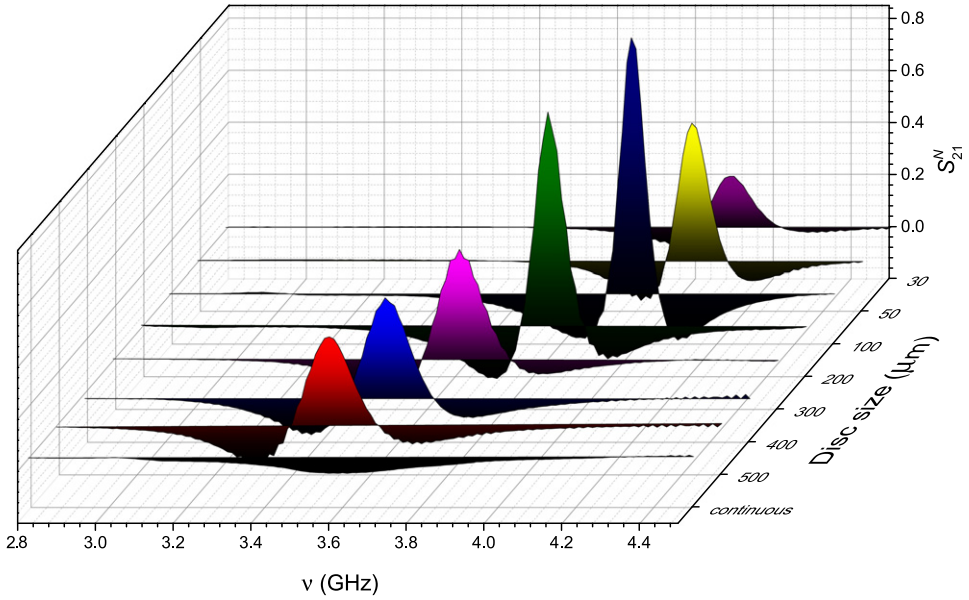

Figure 4. Effect of patterned NiFe element size on hybrid resonance. Scans of S_{21}^N versus ν, taken across an SRR/FMR anticrossing for different disk sizes. The scans were taken in a fixed field $B_a = B_{co}$ (~0.01 T) and normalized to a scan taken at 0.25 T (far away from B_{co}). The shifts in peak position are due to the patterned films having slightly different capacitances, which shifts the position of the SRR resonance [46, 49] (and hence B_{co}). Note that these results are for the magnetic (asymmetric) mode of the SRR (cf section 2).

5. Conclusions and suggestions for further work

In this work it has been demonstrated that magnetic films fashioned from transition metals can be effectively coupled to metamolecules, as long as the film is patterned to suppress eddy currents. The characteristics of the transition metal based magnetic hybrid metamolecule emulates that obtained using YIG films, but with the huge advantage that metallic films can be grown as multilayers and patterned down to sub-micron length scales, using standard clean-room techniques. This opens up a promising field of hybrid metamaterials research, based on the abundance of magnetic phenomena which can be accessed in transition-metal metallic films (see section 1). Here we have demonstrated giant magnetic modulation of a metamolecule resonance (40 dB) in a planar setup, inherently suited to applications. Indeed, the device can be viewed as a stop-band/passband filter, controllable externally by a magnetic field. The results shown in figure 3 also represent the highest frequency magnetic hybrid metamolecule (17 GHz) reported to date. In practice, it should be possible to increase this frequency substantially by using smaller SRRs and magnetic films with built-in intrinsic anisotropy and/or exchange-bias. Here the required magnetic field can be tailored for specific applications. In addition, it has been noted that SRRs have the potential to enhance magnetic resonance sensing in VNA-FMR, making full use of the huge dynamic range available in VNA/CPW experiments. Finally, we observe that the standard clean room techniques used in this work can easily be extended to create more complex magnetic material-metamolecule multilayers and full planar or 3D metamaterials [17, 42].

Competing financial interests

The authors declare no competing financial interests.

Acknowledgments

J C Nash provided photography support. The authors would like to acknowledge the financial support of the Engineering and Physical Sciences Research Council (UK). SAG gratefully acknowledges funding by the Defence and Security PhD Scheme managed by Dstl.

References

[1] Smith D R, Pendry J B and Wiltshire M C K 2004 *Science* **305** 847
[2] Xu T, Abashin M, Agrawal A, Chau K J and Lezec H J 2013 *Nature* **497** 470
[3] Silveirinha M and Engheta N 2006 *Phys. Rev. Lett.* **97** 157403
[4] Rogacheva A V, Fedotov V A, Schwanecke A S and Zheludev N I 2006 *Phys. Rev. Lett.* **97** 177401
[5] Elser J, Wangberg R, Podolskiy V A and Narimanov E E 2006 *Appl. Phys. Lett.* **89** 261102
[6] Fedotov V A, Mladyonov P L, Prosvirnin S L and Zheludev N I 2005 *Phys. Rev.* E **72** 056613
[7] Alu A and Engheta N 2005 *Phys. Rev.* E **72** 016623
[8] Fedotov V A, Rose M, Prosvirnin S L, Papasimakis N and Zheludev N I 2007 *Phys. Rev. Lett.* **99** 147401
[9] Papasimakis N, Fedotov V A and Zheludev N I 2008 *Phys. Rev. Lett.* **101** 253903
[10] Liu N *et al* 2009 *Nat. Mater.* **8** 758
[11] Landy N I, Sajuyigbe S, Mock J J, Smith D R and Padilla W J 2008 *Phys. Rev. Lett.* **100** 207402
[12] Yang Y J, Huang Y J, Wen G J, Zhong J P, Sun H B and Gorden O 2012 *Chin. Phys.* B **21** 038501
[13] Fedotov V A, Rogacheva A V, Zheludev N I, Mladyonov P L and Prosvirnin S L 2006 *Appl. Phys. Lett.* **88** 091119
[14] Schwanecke A S, Fedotov V A, Khardikov V V, Prosvirnin S L, Chen Y and Zheludev N I 2007 *J. Opt.* A **9** L1
[15] Yu N F *et al* 2011 *Science* **334** 333
[16] Sun S *et al* 2012 *Nano Lett.* **12** 6223
[17] Schurig D *et al* 2006 *Science* **314** 977
[18] Zheludev N I and Kivshar Y S 2012 *Nat. Mater.* **11** 917
[19] Tanaka K, Plum E, Ou J Y, Uchino T and Zheludev N I 2010 *Phys. Rev. Lett.* **105** 227403
[20] Hess O, Pendry J B, Maier S A, Oulton R F, Hamm J M and Tsakmakidis K L 2012 *Nat. Mater.* **11** 573
[21] Zhou J *et al* 2012 *Phys. Rev.* B **86** 035448
[22] Zhang Z *et al* 2012 *Nat. Commun.* **3** 942
[23] Stenning G B G, Bowden G J, Maple L C, Gregory S A, Zheludev N I and de Groot P A J 2013 *Opt. Express* **21** 1456
[24] Kang L, Zhao Q, Zhao H and Zhou J 2008 *Opt. Express* **16** 8825
[25] Huang Y J, Wen G J, Li T Q and Xie K 2010 *J. Electromagn. Anal. Appl.* **2** 104
[26] Zhao H, Zhou J, Zhao Q, Li B, Kang L and Bai Y 2007 *Appl. Phys. Lett.* **91** 131107
[27] Gollub J N, Chin J Y, Cui T J and Smith D R 2009 *Opt. Express* **17** 2122
[28] Bi K, Zhou J, Zhao H, Lui X and Lan C 2013 *Opt. Express* **21** 10746
[29] Ghalibafan J, Komjani N and Rejaei B 2012 *J. Electromagn. Waves and Appl.* **26** 914
[30] Huang Y J, Wen G J, Yang Y J and Xie K 2012 *Appl. Phys.* A **106** 79
[31] Rodrigue G P 1988 *Proc. IEEE* **76** 121
[32] Harris V G *et al* 2009 *J. Magn. Magn. Mater.* **321** 2035

[33] Martín F, Falcone F, Bonache J, Marqués R and Sorolla M 2003 *IEEE Microw. Wireless Compon. Lett.* **13** 511
[34] Falcone F, Martín F, Bonache J, Marqués R and Sorolla M 2004 *Microw. Opt. Technol. Lett.* **40** 3
[35] Gil I, Bonache J, García-García J and Martín F 2006 *IEEE Trans. Microw. Theory Tech.* **54** 2665
[36] Lenk B, Ulrichs H, Garbs F and Münzenberg M 2011 *Phys. Rep.* **507** 107
[37] Kruglyak V V, Demokritov S O and Grundler D 2010 *J. Phys. D: Appl. Phys.* **43** 264001
[38] Kittel C 1948 *Phys. Rev.* **73** 155
[39] Kuanr B, Celinski Z and Camley R E 2003 *Appl. Phys. Lett.* **83** 3969
[40] Acher O 2008 *J. Magn. Magn. Mater.* **320** 3276
[41] Simons R N 2004 *Coplanar Wavegude Circuits Components and Systems* (New York: Wiley)
[42] Liu N, Guo H, Fu L, Kaiser S, Schweizer H and Giessen H 2008 *Nat. Mater.* **7** 31
[43] Beaujour J M L, Kent A D, Abraham D W and Sun J Z 2008 *J. Appl. Phys.* **103** 07B519
[44] Zagorodnii V V, Hutchinson A J, Hansen S, Chen J, Gatzen H H and Celinski Z 2010 *J. Appl. Phys.* **107** 3906
[45] Kuhlmann N, Vogel A and Meier G 2012 *Phys. Rev.* B **85** 4410
[46] Baena J D *et al* 2005 *IEEE Trans. Microw. Theory Tech.* **53** 1451–61
[47] Zhou J, Koschny T and Soukoulis C M 2007 *Opt. Express* **15** 17881
[48] Huebl H *et al* 2013 *Phys. Rev. Lett.* **111** 127003
[49] Zhu W, Yongjun H, Rukhlenko I D, Wen G and Premaratne M 2012 *Opt. Express* **20** 6616